Journal of Applied Electrochemistry **33**: 51–59, 2003.

Electrochemical detection of large channels in porous rocks

S.O. ENGBLOM[1,2], J.C. MYLAND[1], K.B. OLDHAM[1,*], A.L. TAYLOR[1,3] and W.C. TOPIC[1,4]
[1]*Department of Chemistry, Trent University, Peterborough, Ontario Canada K9J 7B8*
[2]*Present address: Swedish University of Agricultural Science, S-750 07 Uppsala, Sweden*
[3]*Present address: Department of Dentistry, University of Western Ontario, London, Canada*
[4]*Present address: Department of Chemistry, University of Alberta, Edmonton, Canada*
*(*author for correspondence, fax: 1 705 748 1625, e-mail: koldham@trentu.ca)*

Received 1 October 2001; accepted in revised form 12 June 2002

Key words: conductance, pore-size, porosity, porous rocks

Abstract

An electrochemical method for studying channels in porous rocks and similar insulators, has been developed. In principle, the method consists of displacing a nonconducting liquid from the pores by an inflow of an ionically conducting solution. The conductance is monitored continually as the rate of flow through the rock is gradually increased. The rate of conductance increase is interpreted in terms of a simple model, based on Poiseuille flow through a capillary network, to provide information about the sizes and numbers of large pores in the rock. Three rock samples have been analysed.

1. Introduction

The extent and the configurations of the voids in porous rocks are of vital interest in a number of contexts. It is in the pores of petroleum reservoir rocks that the hydrocarbons reside. Likewise ground water resources generally occupy the pores of aquifer rocks. In both these instances, the volume of imbibed liquid is beneficially larger when the pores are large and numerous. In contrast, when one is seeking a rock stratum to provide containment for radioactive waste or other pollutants, then the presence of pores or fissures is undesirable.

The total void volume is not, in itself, a particularly useful measure of the fitness of a porous rock for a specific purpose. Totally isolated voids are innocuous and blind-ended passageways are of little concern. Interest is primarily in the interconnected spaces that communicate with each other and, ultimately, with the exterior. It is these spaces that are usually associated with the word 'pore'.

The number and sizes of the pores and other voids determine the rock's porosity, that is, the fraction of the total volume that is not rock. The diameter of a pore is a very strong determinant of its contribution to the flow of a fluid through a porous medium. Because of their compressibility, gases obey different equations of motion than liquids and it is the latter that will be our concern here. Liquids flow through a smooth pore with a velocity that is, at least approximately, proportional to the square of the pore's diameter and, since the volume flow is also proportional to the cross-sectional area of the pore, it is the *fourth* power of the pore's diameter that determines its volumetric transporting capability. This emphasizes the disproportionate importance of *large* pores. The tortuosity of the pores is also important. These factors underline the equal importance of porosity and of pore-size distribution in characterizing a rock: porosity governs the liquid-holding capacity of a rock; pore-size distribution controls the movement of the liquid through the rock.

The methods that have been used to study porous materials, including rocks, are legion. Sectioning the rock, followed by micrography, is one very direct method of observing pore structure. Another, which has even been applied to rocks, is to polymerize a plastic or solidify an alloy inside the pores and then dissolve away the matrix itself. Gas adsorption isotherms are commonly measured [1]; these provide access to the internal area of the sample. Intrusion porosimetry [2] involves progressively squeezing a liquid, usually mercury, into the pores. In this popular method, the volume against pressure characteristic can be interpreted as a distribution of pore sizes, because the smaller the pore, the more pressure is needed to overcome the surface tension resisting the intrusion. Of course, the most direct way of studying the flow of liquids through porous rock is to measure the rock's permeability under closely controlled conditions and many such permeametric studies are conducted routinely. Under the curious name of 'formation factor' measurement, the porosity of materials has sometimes been investigated electrochemically [3] by a method that is essentially as described

below in Section 6. We have employed other electrochemical approaches [4–8] in the study of porous media. These make use of the diffusion and/or migration of particular ions through the pores to provide information, via an electric current, on the nature of the paths that the ions follow.

The principle behind the present method, described in more detail in later Sections, is easily understood. The pores of a rock sample are filled with a nonconducting liquid. Then a conducting liquid is caused to flow through the rock, displacing the nonconductor. In the early phases of the experiment, the sample remains nonconducting, but as soon as the first trace of conductor reaches the other side of the sample, a measurable electrical conductance is observed. This initial 'breakthrough' will be due to the largest pore because, the larger the pore, the faster the flow through it. As time passes, more and more breakthroughs occur and the conductance steadily increases. With the aid of a model, the way in which the conductance increases during the experiment can be used to express the distribution of pore sizes in the rock.

2. The model

Let it be made clear that we are in no way suggesting that the model we adopt comes close to representing the pores in any actual rock sample. A truly realistic model would incorporate so many parameters as to defy any useful mathematical representation. Our model has been chosen for mathematical tractability, not for realism. Nevertheless, we believe that our naïve model captures some of the essential characteristics of the pores of an rock sample, from the viewpoint of liquid permeation through the rock.

Our model is 'capillaric' in nature: it regards the permeance of the rock as arising from distinct passageways. Models that treat porous materials as a collection of discrete one-dimensional tubules can be and have been criticized (e.g. [3], p.169) and such a criticism is valid. Nevertheless, we see no tractable alternative for our present purpose.

The rock sample has two parallel faces and we envisage many pores to traverse the sample from one face to the other. There will be pores heading in other directions and they will contribute to the porosity of the rock but, unless they open onto both end faces, they are of no concern in the present analysis. The pores that contribute to transport in the direction perpendicular to the parallel faces will be described as 'axial pores'. Three such pores are shown in Figure 1. Of course some pores will intersect others, but such junctions have a minor bearing on the transport properties and in our model there is no recognition of pore intersection. As depicted in Figure 1, each pore is treated as a long one-dimensional tubule, essentially cylindrical in shape, with a diameter d_j that varies from one pore to the next, though not within a single pore. All axial pores are regarded as having the same length that is longer than the direct route from one face to the other by a common tortuosity factor λ. We shall later ascribe a value of 2 to this uniform tortuosity. It is convenient to assign an integer index j to each axial pore, ordered so that $j = 1$ corresponds to the widest pore, $j = 2$ to the next widest, and so on.

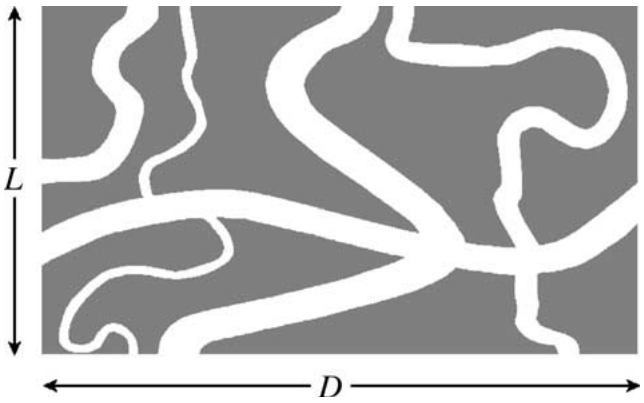

Fig. 1. The simplistic model of the pore structure of rocks on which our analysis is based. All axial pores, of which three are shown, are assumed to have the same length λL and the jth pore has a uniform cross-sectional area $\pi d_j^2/4$.

The most unrealistic feature of our model is the treatment of the pores as of uniform diameter. Attempts to formulate a model that incorporated a length-dependent area were not successful. The d_j term represents some sort of average of what in reality must be a very variable diameter.

3. The samples

We have studied three samples of porous rock of different types: a dolomite (sample L), a siltstone (sample Z) and a limestone (sample C). Each porous rock, received as part of a drill core, was machined to the shape of a squat cylinder of diameter D (about 4 cm) and height L (about 3.5 cm). The sample was mounted in shrink-wrap tubing and thoroughly cleaned by forcing, under vacuum, first ethanol, then acetone and finally water through its pores.

After drying in a vacuum oven for 8 h, the sample was allowed to cool overnight in a desiccator and weighed. Next, the sample was left in an evacuated chamber for one hour; then, still under vacuum, it was submerged in degassed water and left overnight. After breaking the vacuum next morning, and blotting away the surface water, the rock was reweighed. These entire procedures were repeated several times until concordant values were obtained of the sample's dry mass m_{dry} and its mass, m_{wet}, after water imbibition. Making use of the density of water, we calculated the total porosity as

$$\theta = \frac{4(m_{\mathrm{wet}} - m_{\mathrm{dry}})}{\pi D^2 L \rho_{\mathrm{H_2O}}} \tag{1}$$

This is the 'imbibition method' of determining porosity; other methods are discussed and classified by Scheidegger [9]. θ does not appear in the theory of our method, but it provides a basis for comparison of our results. Moreover, we regard this quantity as important for characterizing the rock. For a similar reason, the formula

$$\rho_{\text{rock}} = \frac{4m_{\text{dry}}}{\pi(1-\theta)D^2L} \tag{2}$$

was employed to calculate the apparent density of the rock matrix. The values of these physical properties, with standard deviations calculated from repeated measurements, for the three rock samples that were investigated in this study, are assembled in Table 1, together with other data. Of course, the presence of isolated voids will undermine the measurements of both θ and ρ_{rock}.

After physical characterization, the cylindrical rock sample was cemented into the base of an acrylic pipe, the inner diameter, $D_{\text{pipe}} = 37.77$ mm, of which was enlarged slightly at its lower end to accommodate the rock. The pipe, about 2 m in length, was fitted with a small nipple, level with the upper surface of the rock, as illustrated in Figure 2.

We can distinguish between the total porosity θ of the rock and the axial, or effective, porosity θ_{axial}, which is the porosity of those pores which contribute to flow through the rock in the axial (vertical) direction. In terms of our model, the latter is the ratio of the void volume of the axial pores to the overall volume, being given by

$$\theta_{\text{axial}} = \frac{\sum_j \pi d_j^2 \lambda L/4}{\pi D^2 L/4} = \frac{\lambda}{D^2}\sum_j d_j^2 \tag{3}$$

4. The apparatus

Nickel gauze electrodes are positioned in contact with the upper and lower faces of the rock sample. As illustrated in Figure 2, the upper electrode is a disc of diameter slightly less than that of the rock; it is positioned inside the pipe and is welded at its centre to a stout nickel lead. This lead is centrally mounted and is long enough to protrude from the top of the pipe,

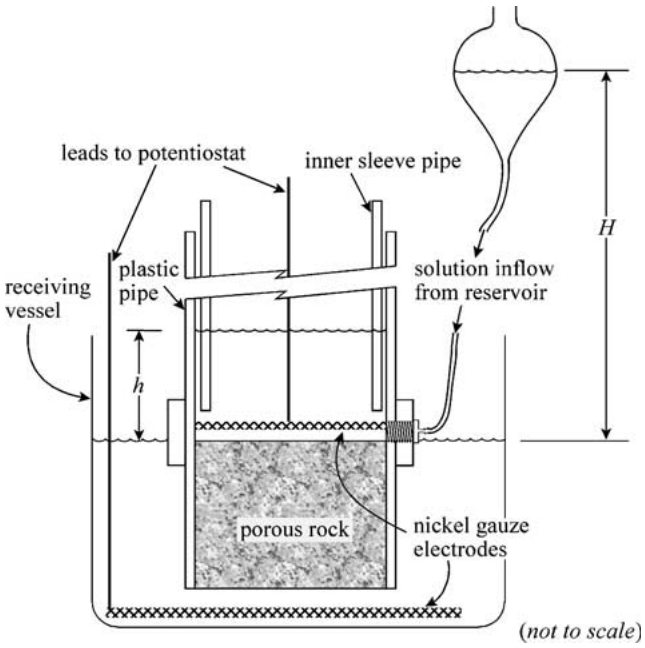

Fig. 2. Exploded cross-sectional diagram of the apparatus.

whereby electrical contact can be made. To ensure closer contact with the upper rock surface, the upper disk is pressed down by the weight of a plastic 'sleeve' pipe, of about 3 cm internal diameter, which fits inside the main pipe. The pipe assembly is positioned vertically and rests on the lower gauze electrode, a disc of about 5 cm diameter. This lower gauze is mounted on a nickel sheet, to which a second nickel lead is welded at its perimeter, and which itself rests on the floor of the flat–bottomed receiving vessel, as clarified in Figure 2. A salient quantity in the theory of operation is the area A of the liquid–air interface in the pipe. This is somewhat less than $\pi D_{\text{pipe}}^2/4$ because of the space occupied by the sleeve pipe and, to a minor extent, by the nickel lead wire. In fact, in a self-evident notation:

$$A = \frac{\pi}{4}[D_{\text{pipe}}^2 - (D_{\text{outer}}^2 - D_{\text{inner}}^2)_{\text{sleeve}} - D_{\text{wire}}^2] \tag{4}$$

Its value in all our experiments was 793.4 mm^2.

To minimize air entrapment, outgassed solutions were drawn up through the rock, under suction, to 'prime' the rock channels. Thereafter, liquids poured into the top of the pipe will, under the gravitational force provided by a head, slowly permeate through the rock and enter the receiving vessel. In some experiments only a small

Table 1. Model-independent characteristics for three rock samples

	L (dolomite)	Z (siltstone)	C (limestone)
Diameter, D/mm	38.02 ± 0.32	38.96 ± 0.04	37.80 ± 0.08
Height, L/mm	32.61 ± 0.16	42.08 ± 0.07	35.87 ± 0.05
Mass, m_{dry}/g	91.501 ± 0.005	113.72 ± 0.11	92.535 ± 0.012
Porosity, θ	0.105 ± 0.003	0.1233 ± 0.0004	0.1692 ± 0.0010
Density, ρ_{rock}/kg m^{-3}	2760 ± 70	2586 ± 13	2767 ± 16
$4LG/\pi D^2\kappa = \theta_{\text{axial}}/\lambda^2$	0.014		0.036

volume of liquid was poured into the pipe and the level in the receiving vessel was adjusted to match that in the pipe, so that flow was inhibited. More often, the liquid level in the receiving vessel was aligned with the upper surface of the rock. The nipple allows an alternative route by which liquids can be introduced into the pipe. When the nipple is in use, a long (about 10 m) length of narrow bore (nominally 1.59 mm internal diameter) plastic tubing connects it to a reservoir vessel mounted high enough to deliver liquid onto the top surface of the rock at a suitable rate. The height H of the meniscus in this reservoir above the upper surface of the rock was maintained at close to 1.802 m in most of our experiments.

The aqueous liquids used were degassed to deter the formation of air bubbles inside the rock pores. Once brought into use, it is preferable that the rocks never be allowed to dry out, though this did, on occasion, foster the growth of biota on the rock's surface.

The electrical leads from the two gauze electrodes are connected to an Australian-built instrument [10] designed to measure the interlead impedance. This equipment applies twenty-four a.c. frequencies, ranging from 49.95 Hz to 7.855 kHz, simultaneously, the voltage amplitude of each being 5.0 mV. The resulting multi-frequency current is measured and Fourier transformed automatically by the instrument, whereby the in-phase and out-of-phase impedances, Z' and Z'' can be determined and plotted against the reciprocal of the frequency. A typical graph is shown in Figure 3. The in-phase impedance is almost frequency-independent and the value extrapolated to infinite frequency, $Z'(\infty)$, is regarded as the electrical resistance R encountered between the nickel gauze electrodes, that is, the resistance of the liquid in the pores of the rock. In contrast, Z'' is always small and negative: it is associated with the double-layer capacitance at the nickel gauze electrodes, a matter of no concern in this study. In terms of our model, the measured resistance R is the resistance of all the axial pores in parallel. Of more relevance in the theory is the conductance G of the liquid occupying the pores. The total conductance, the reciprocal of the resistance, is the sum of the individual conductances of all the axial pores. If g_j is the conductance of the jth pore, then

$$\frac{1}{Z'(\infty)} = \frac{1}{R} = G = \sum_j g_j = \frac{\pi\kappa}{4\lambda L}\sum_j d_j^2 \tag{5}$$

according to our model. In the final step of this chain of equalities, we assume the conductance within each pore to be proportional to the cross-sectional area of the pore (regarded as circular) and to the conductivity κ of the liquid that fills it, but inversely proportional to the pore's length λL. Equation 5 is the electrochemical basis of the preliminary experiments reported below: it applies when all the axial pores are entirely filled with a liquid of uniform conductivity.

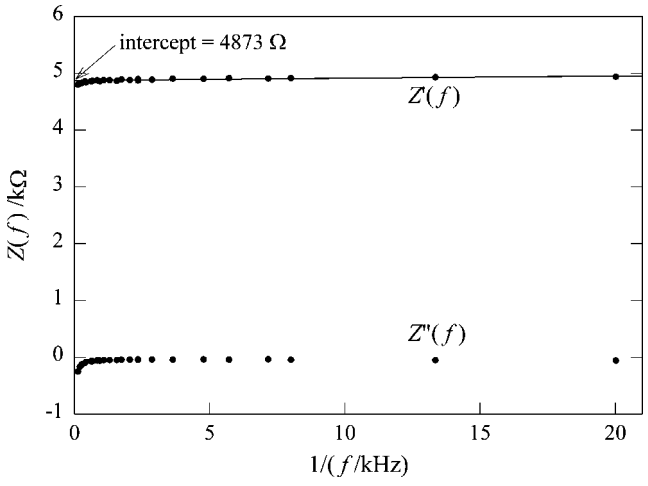

Fig. 3. Typical impedance plot.

5. Hydraulic considerations

The permeability P of a porous material is defined, on the basis of Darcy's Law, as the volume rate of flow of a liquid of unit viscosity through unit area of the material when a unit pressure differential exists across unit thickness of the material. The dimensions of P are those of area. According to Darcy's law the volume flow rate though our rock sample is

$$\frac{\mathrm{d}V}{\mathrm{d}t} = \frac{-P_{\mathrm{rock}}}{\eta}\frac{\pi D^2}{4}\frac{\Delta p}{L} \tag{6}$$

where V denotes the volume of the liquid, of viscosity η, in the pipe. In our experiments, the pressure differential is provided by a head h of the liquid in the pipe and therefore $\Delta p = \rho g h$ where g is gravitational acceleration and ρ is the liquid's density. In our preliminary experiments, the flow of liquid through the rock is accompanied by a decrease in the level of liquid in the pipe, so that $\mathrm{d}V = A\mathrm{d}h$ where A, defined in Equation 4, is the effective cross-sectional area of the pipe. With these substitutions, Equation 6 becomes

$$\frac{\mathrm{d}h}{\mathrm{d}t} = \frac{1}{A}\frac{\mathrm{d}V}{\mathrm{d}t} = \frac{-P_{\mathrm{rock}}}{\eta}\frac{\pi D^2}{4A}\frac{\rho g h}{L} \tag{7}$$

In our pore-size experiments the hydraulic situation is somewhat more complicated than that described above. Liquid is being fed via the narrow plastic tube and introduced into the pipe through the nipple. Because we adjust the inflow of liquid by this route to be initially much greater than the outflow through the rock, the head in the pipe rises, rather than falls. The inflow rate is proportional to $H - h$, where H is the height of the reservoir vessel meniscus above the upper surface of the rock. Thus, analogously with Equation 7,

$$\frac{\mathrm{d}h}{\mathrm{d}t} = \frac{1}{A}\frac{\mathrm{d}V}{\mathrm{d}t} = \frac{k(H-h)}{A} - \frac{\pi D^2 \rho g}{4\eta A L}P_{\mathrm{rock}}h \tag{8}$$

where k is the proportionality constant between flow-rate through the narrow tube and head. This constant could have been estimated via Poiseuille's law but we chose to measure it instead. With the boundary condition $h = 0$ at $t = 0$, differential Equation 8 may be integrated to

$$\ln\left\{1 - \left(1 + \frac{\pi D^2 \rho g P_{\text{rock}}}{4\eta L k}\right)\frac{h}{H}\right\} = -\left(\frac{k}{A} + \frac{\pi D^2 \rho g P_{\text{rock}}}{4\eta A L}\right)t \tag{9}$$

Early data from an experiment with a rather impermeable rock display no detectable curvature when $\ln((H - h)/H)$ is plotted against t, indicating that the contribution of the terms containing P_{rock} was negligible. From the slope we calculated $k = 0.1365$ mm^2 s^{-1}.

Irrespective of the permeability of the rock, Equation 9 may be inverted and rephrased as

$$h = \frac{kHT}{A}\left[1 - \exp\left(\frac{-t}{T}\right)\right] \tag{10}$$

where T is the hydraulic time constant of the experiment, defined by

$$T = \frac{A}{k + \dfrac{\pi D^2 \rho g P_{\text{rock}}}{4\eta L}} \tag{11}$$

A typical value of this time constant in our experiments was 1.5 h.

6. Preliminary electrochemical experiments

The liquids used in our experiments were invariably solutions of potassium chloride of various concentrations (including zero) in reverse-osmosis purified water that were degassed under vacuum, with stirring, prior to use. No attempt was made to prepare solutions of accurately known concentration, because the solutions were characterized by their conductivities, which were measured by an Orion (model 150) conductivity meter. Thus the c values in Table 2 are approximate only. The experiments described in this Section were all performed with concentration uniformity, that is, the aqueous solutions in the pipe, in the rock pores, and in the receiving vessel were all of ostensibly identical composition. These experiments were carried out to confirm some of the basic premises on which the pore-size experiments, described later, rest.

Table 2. Rock conductance against solution conductivity data for rock sample L

Concentration, c/mM	Conductivity, κ/S m^{-1}	Conductance, G/mS	(G/κ) /mm
30	0.399	1.590	0.398
100	1.350	0.5930	0.439
10	0.1461	0.07369	0.504
30	0.403	0.2024	0.502
100	1.281	0.6000	0.468
300	3.62	1.678	0.463
1000	11.08	5.140	0.464
300	3.65	1.796	0.492

We argued that the conductance of a solution-filled rock sample should be (a) proportional to the conductivity κ of the imbibed solution and (b) independent of whether, and how fast, the solution might be flowing through the rock. Postulate (b) was easily confirmed by observing no measurable change in the measured conductance G when the head h was varied or zeroed.

Table 2 shows the results of experiments on rock L, designed to verify postulate (a) by investigating the constancy of the G/κ ratio, when the rock was filled with a sequence of solutions of various concentrations. Such experiments are lengthy, because it takes a very long time to completely flush one solution from the rock by flowing a second solution through. Often, solutions were allowed to flow for one week or more between measurements. Though the constancy is not outstanding, the ratio of G/κ shows no confident trend with concentration. The table is ordered to match the chronology of the experiments and it should be noted that there is a strong tendency for the measured ratio to be higher when the new solution was more dilute than the solution it replaced. For rock Z, we failed to verify postulate (a), probably because it was impractical to flush this sample for the length of time that would have been needed.

The quantity $\pi\kappa D^2/4GL$ is the ratio of the resistance of the soaked sample to the resistance of a similarly sized volume of the conducting liquid: this is the quantity known in the literature as the 'formation factor' (see [3], p. 245). Measured values of the reciprocal of this quantity are included in Table 1 for rocks L and C. The G/κ value during these preliminary experiments has a simple interpretation in terms of our model. Straightforward combination of Equations 5 and 3 produces

$$\frac{G}{\kappa} = \frac{\pi D^2}{4L}\frac{\theta_{\text{axial}}}{\lambda^2} \tag{12}$$

Thus, the numbers listed in the final row of Table 1 may be associated with the effective porosity of the rock sample, divided by the square of the tortuosity. Despite the crudity of our model, it is apparent that an interpretation of the tabulated numbers as the term $\theta_{\text{axial}}/\lambda^2$ is quite credible. For, with our heuristic assumption that the tortuosity $\lambda = 2$, one calculates a $\theta_{\text{axial}}/\theta$ ratio of 0.85 for rock C and 0.52 for rock L, neither of which is unreasonable.

7. Pore-size experiments

Each of these experiments commenced with the rock sample soaked with pure water, but without any overlying unimbibed water. This condition was achieved

by leaving water flowing from the filled pipe and through the rock for many days, then allowing the dregs to escape through the nipple. After the level in the receiving vessel was adjusted to match the rock's upper surface, and measuring the initial conductance $G(0)$, the experiment was ready to begin.

At $t = 0$, the nipple was connected to the long narrow plastic tube and a concentrated (usually either 0.1 or 1 M) solution of potassium chloride was allowed to flow slowly onto the upper surface of the rock. The flow through the rock, zero at $t = 0$, builds up steadily as the head increases, in obedience to Equation 10. The increasing head is an important feature of these experiments because it lengthens the effective time-span of the experiment. In earlier studies [11] we had imposed a constant head, but that did not provide an efficient way of discriminating between pores of different large sizes.

The conductance $G(t)$ was measured at intervals as frequent as one minute for a period of several hours. Figure 4 shows typical results. As well, the height $h(t)$ was monitored. Two other tasks that require periodic attention during an experiment are the maintenance of a constant head H in the elevated reservoir and ensuring that the liquid level in the receiving vessel remains in register with the upper surface of the rock.

Rough calculations show that the conductance of a rock sample filled with absolutely pure water, and attributable to the H_3O^+ and OH^- ions present, should have been less than 0.1 μS (or $R > 10$ MΩ), but we never achieved $G(0)$ readings anywhere nearly as low this, 10 μS being more typical. In the flushing period prior to a pore-size experiment, the conductance gradually decreases, but it would have been necessary to leach ions for several years before the conductance approached that of the flushing water. Nevertheless, the conductivity distinction between the outgoing 'water' and the incoming concentrated salt solution was sufficient to validate the principles of the method.

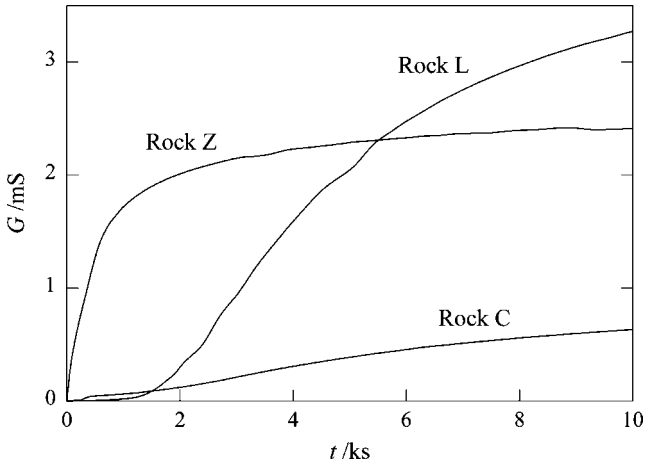

Fig. 4. Experimental conductance against time graphs for the three rock samples. At time zero, the rocks are saturated with water, but thereafter solutions of potassium chloride flow through the rocks at an ever increasing rate. The conductivities of the solutions were: 1.257 S m^{-1} for rock C; 10.84 S m^{-1} for rock L and 1.249 S m^{-1} for rock Z.

8. Theory of the pore-size method

Though there are several processes that will lead to local mixing, we assume that the front between incoming solution and the outgoing water is maintained distinct as the front moves through an axial pore. It is also assumed that water and aqueous solutions flow through the jth pore in accordance with the Poiseuille equation. That is,

$$\frac{\mathrm{d}v_j}{\mathrm{d}t} = \frac{\pi d_j^4}{128\eta}\left(\frac{\mathrm{d}p}{\mathrm{d}\ell}\right)_j \tag{13}$$

where v_j denotes the volume of new liquid in the axial pore and ℓ is a length coordinate measured along the pore, with its origin at the pore entrance. The pressure gradient along the jth axial pore is denoted by $(\mathrm{d}p/\mathrm{d}\ell)_j$ and can be equated to $\rho gh/\lambda L$. The speed of the advancing front along this pore, $\mathrm{d}\ell_j/\mathrm{d}t$, equals $(4/\pi d_j^2)(\mathrm{d}v_j/\mathrm{d}t)$, and accordingly

$$\frac{\mathrm{d}\ell_j}{\mathrm{d}t} = \frac{\rho g h d_j^2}{32\eta\lambda L} \tag{14}$$

Note that no distinction is being made between the viscosity of the KCl solution and that of pure water. Nor shall we distinguish between the densities of those liquids. The ratio η/ρ is known as the liquid's kinematic viscosity, that will be denoted here by $\tilde{\eta}$. Next, rearrangement and formal integration of Equation 14 lead to

$$\int_0 \mathrm{d}\ell_j = \frac{g d_j^2}{32\tilde{\eta}\lambda L}\int_0 h\,\mathrm{d}t \tag{15}$$

Equation 15 refers to a single axial pore and is valid only at times short enough that the water/solution front is still contained within the pore. Initially and approximately, the head h varies linearly with time as is demonstrable from Equation 9 or 10. These equations could be used to perform an analytical evaluation of the right-hand integral in Equation 15, but we preferred to use experimental h against t data.

Let us use the term 'pore transit time' and the symbol t_j to denote the time that it takes for the front, moving along the coordinate ℓ_j, to reach the lower end of the jth axial pore. Since our model treats water as of zero conductivity, the measured conductance of the rock is predicted to remain at zero until the instant $t = t_1$ at which the salt solution penetrates to the exit of the widest pore. The conductance will then jump to

$$G(t_1 \leqslant t < t_2) = g_1 = \frac{\pi\kappa d_1^2}{4\lambda L} \tag{16}$$

and remain at that value until the next widest pore also becomes filled with solution. This behaviour is evident for rock L in Figure 4, though not for rock Z, for which t_1 is immeasurably small in our experiments. At all times beyond t_1, there will be some pores which are 'filled'

with KCl solution, the remainder will be 'filling'. Each filled axial pore will contribute its constant conductance to that of the rock, the filling ones will contribute nothing. To obtain a general expression for the transit time t_j, we use it as the upper limit of the right-hand integral of Equation 15 and simultaneously insert λL as the upper limit of the left-hand integral. Performing the integrations then gives

$$d_j^2 = \frac{32\tilde{\eta}\lambda^2 L^2}{g\int_0^{t_j} h\mathrm{d}t} \tag{17}$$

after rearrangement. A pore of diameter d_j given by this equation achieves breakthrough at a time t_j. Approximately, the integral equals $kHt_j^2/2A$ initially, so that the $t_j d_j$ is seen to be roughly constant. Note that we assume no interference from adsorption of ions on the walls of the pores, or of other modes of conductance, other than arising from the three-dimensional mobility of ions. Further, our assumption that the liquid in a pore has a segment with no conductivity followed by a solution-filled segment with uniform conductivity κ, means that our results are not valid at very long times. As an experiment proceeds, there is time for both diffusion and convection to cause mixing, blurring the solution front as it moves through a pore. Because of this, our data become increasingly unreliable as time progresses. Accordingly, quantitative analysis of the experimental data will be confined to short times in Figure 5.

Because we are dealing with a large number of pores, it is legitimate to move the discussion from a discrete to a continuous distribution of pores. Let $n(d)$ denote the number of axial pores that have diameters greater than or equal to d so that $n(d_1)$ equals 1, d_1 being the diameter of the largest pore. The number of pores with diameters between d and $d + \mathrm{d}d$ is

$$n(d) - n(d + \mathrm{d}d) = \mathrm{d}n \tag{18}$$

Each pore in this small cohort of axial pores has a conductance of $\pi\kappa d^2/4\lambda L$ and therefore, if $\mathrm{d}G$ is the total conductance of the cohort

$$\mathrm{d}G = \frac{\pi\kappa d^2}{4\lambda L}\mathrm{d}n \tag{19}$$

In the time interval $\mathrm{d}t$, the increase in total conductance is, according to our model, due solely to the cohort of pores that achieves breakthrough in that time interval because those that are already filled do not change their contribution, and the contributions of those that have yet to fill are deferred. Because the treatment is now of a continuum of pores, we may ignore the subscript j's in Equation 17, which thereby describes a one-to-one relationship between time t and the diameter d of the pores that are breaking through at that time. This permits Equation 19 to be rewritten as

$$\frac{8\pi\tilde{\eta}\kappa\lambda L}{g}\mathrm{d}n = \mathrm{d}G\int_0^t h\,\mathrm{d}t \tag{20}$$

The same one-to-one relationship allows Equation 20 to be integrated by specifying time limits on the right-hand side and the corresponding diameter limits on the left:

$$\frac{8\pi\tilde{\eta}\kappa\lambda L}{g}\int_{d_1}^{d}\frac{\mathrm{d}n}{\mathrm{d}d}\mathrm{d}d = \int_{t_1}^{t}\mathrm{d}G\int_0^t h\,\mathrm{d}t \tag{21}$$

Integration of the right-hand side is accomplished by parts; the left-hand side integrates as a consequence of the definition of n:

$$\frac{8\pi\tilde{\eta}\kappa\lambda L}{g}n(d) = G\int_0^t h\mathrm{d}t\Big|_{t_1}^{t} - \int_{t_1}^{t} Gh\mathrm{d}t \tag{22}$$

This is the fundamental equation that provides access to the pore-size distribution of the rock sample.

Equation 22 may be written more informatively as

$$n(d) = \frac{g}{8\pi\kappa\tilde{\eta}\lambda L}\left[G(t)\int_0^t h(\tau)\mathrm{d}\tau - \int_0^t G(\tau)h(\tau)\mathrm{d}\tau\right] \tag{23}$$

All the terms in the coefficient $g/8\pi\kappa\eta\lambda L$ have either been measured experimentally or are well known physical quantities, except for the tortuosity λ, to which we accorded the value 2. The experiment provides conductance-and-head-against time data from which numerical values of the bracketed term are available at any chosen time. The $n(d)$ term is thereby calculable and gives the number of pores with diameters exceeding d which, as Equation 17 shows, is the number of pores with diameters exceeding

$$d = \lambda L\sqrt{\frac{32\tilde{\eta}}{g\int_0^t h(\tau)\mathrm{d}\tau}} \tag{24}$$

which is also calculable at the chosen time. Notice that time serves as a parameter that is absent in the final analysis. Results obtained by this procedure are presented in Figure 5 for the three rocks and will be analysed in the next section.

9. Results of pore-size experiments

Figure 4 shows examples of the raw conductance against time data. Note the marked distinction between the behaviours of rocks L and Z. The latter shows an immediate rise in conductance whereas the former remains insulating for about 1 ks. Our interpretation of this distinction is that there are pores in rock Z that

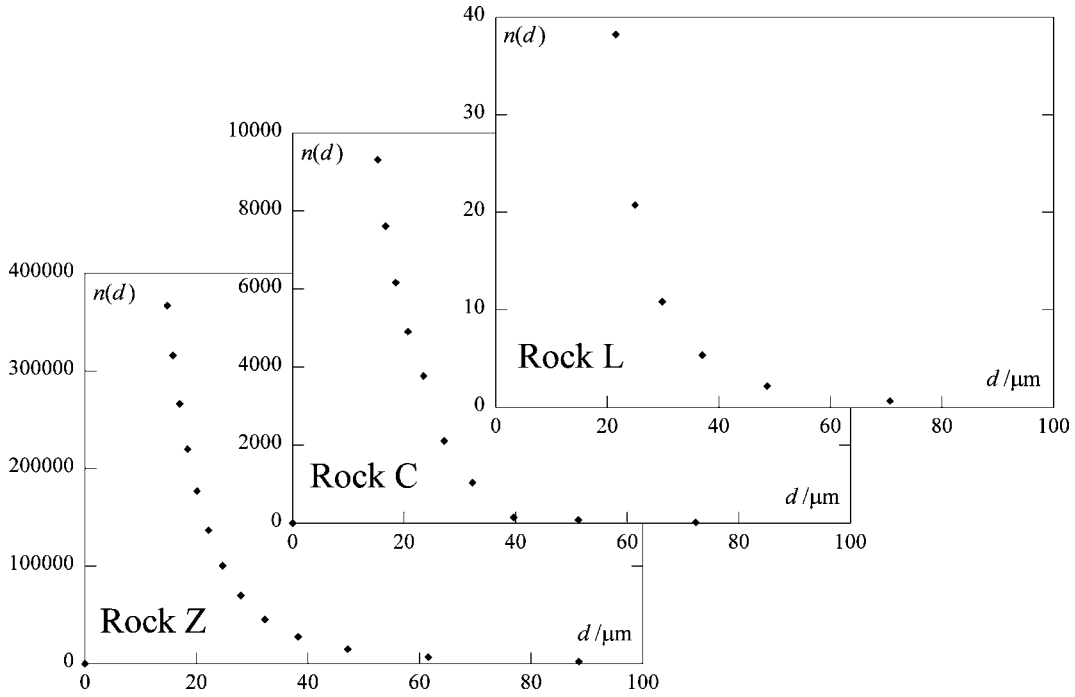

Fig. 5. Plots of $n(d)$, the number of pores with diameters greater than or equal to d, against d.

Table 3. Total pore areas of pore-diameter cohorts for three rock samples

Range of pore diameters /μm	Rock L /mm^2	Rock Z /mm^2	Rock C /mm^2
>50	0.01	65	0.39
20–50	0.028	105	3.2
10–20	0.099	101	2.7
5–10	1.63	111	7.5
>5	1.77	382	13.8
2–5	16.7	–	31
1–2	19.9	–	40
>1	38	–	85

allow the transit of solution before a measurement could be taken. Evidently, rock L lacks pores of a size that allow transit for many minutes. The behaviour of rock C is intermediate. This qualitative interpretation of Figure 4 is model-independent, but our quantification of these results relies on the (imperfect) model discussed in previous sections.

Using trapezoidal approximations for the integrals, the conductance-and-height against time data were processed through Equations 23 and 24 to produce the graphs displayed in Figure 5. Though all three curves are of similar shape, note the wide variation in the ordinate ranges. If we interpret the graphs literally, then rock L has 50 pores with diameters exceeding 20 μm, the corresponding numbers for rocks C and Z being 5300 and 180 000, respectively.

Another way of viewing the size distribution is in terms of the areas occupied by pores of a particular range of diameters. Therefore we used the data from which Figure 5 was generated to calculate

$$\frac{\pi}{4}\int_{d=d_{\mathrm{II}}}^{d=d_{\mathrm{I}}} d^2 \mathrm{d}n \tag{25}$$

for round values of d_{I} and d_{II}. The results of these calculations are shown in Table 3 for each of the three rocks. Notice the large disparity among the three. However, in all cases small pores contribute a majority of the total area despite their small individual areas. The table also includes the aggregated area for rock samples C and L and we can use those values to estimate the effective, or axial, porosities of these samples by using Equation 3 and ignoring pores of <1 μm diameter. This calculation yields 0.15 for sample C and 0.067 for sample L, corresponding to $\theta_{\mathrm{axial}}/\theta$ ratios of 0.89 and 0.64, respectively, in good agreement with those reported in Section 6. The corresponding calculations for rock Z yield nonsensical results.

10. Discussion

Among the flaws in our model are: the treatment of the pores as distinct tubules; the assumption of uniform pore cross-sectional area; the assumption of a uniform tortuosity of 2; the firm distinction between axial and non-axial pores; the neglect of pore intersection and blind pores; the assumption that ionic adsorption is absent; the assumption of Poiseuille flow and the neglect of mixing of the preexisting insulating solution with the incoming conducting solution.

Despite these flaws, which imply that our results should not be interpreted literally, we believe that the

different distributions that we find for rocks C and L correspond to real differences in the distribution of large pores in those two rocks. Though the overall porosity of rock C is only about 60% greater than that of rock L, our results suggest a much greater preponderance of large pores in rock C. For reasons we don't fully understand, rock Z cannot be interpreted in terms of our model.

Acknowledgements

We are grateful to Ken Fowler for his technical skill in constructing parts of the apparatus. The financial aid of the Natural Sciences and Engineering Research Council of Canada is gratefully acknowledged. Early phases of this study were supported by a generous grant from Imperial Oil.

References

1. A.W. Adamson, 'Physical Chemistry of Surfaces' (John Wiley & Sons, New York, 3rd edn, 1976), chapter 14.
2. J. van Brakel (ed.), *Powder Technol.* **29** (1981) 1–209.
3. F.A.L. Dullien, 'Porous Media: Fluid Transport and Pore Structure' (Academic Press, San Diego, 2nd edn, 1991), pp. 306–311.
4. K.B. Oldham and L.E. Topol, *J. Phys. Chem.* **71** (1967) 3007.
5. L.E. Topol and K.B. Oldham, *J. Phys. Chem.* **73** (1969) 1455.
6. K.B. Oldham and L.E. Topol, *J. Phys. Chem.* **73** (1969) 1462.
7. M.G. Kamau, J.C. Myland and K.B. Oldham, Proceedings of the international conference on 'Porous Media and their Applications in Science, Engineering and Industry', Kona, Hawaii, (1996), p. 433.
8. J.C. Myland, K.B. Oldham, J. Schiewe and A.L. Taylor, *Can. J. Chem.* **76** (1998) 1688.
9. A.E. Scheidegger, 'The Physics of Flow through Porous Media' (University of Toronto Press, Toronto, 3rd edn, 1974).
10. J. Hazi, D.M. Elton, W.A. Czerwinski, V.A. Vicente-Beckett and A.M. Bond, *J. Electroanal. Chem.* **437** (1997) 1.
11. J.C. Myland, K.B. Oldham and W.C. Topic, Proceedings of the 'Fractured Rock 2001' conference, Toronto, Ontario (2001).